International Journal of Mass Spectrometry 359 (2014) 26–37

Contents lists available at ScienceDirect

International Journal of Mass Spectrometry

journal homepage: www.elsevier.com/locate/ijms

Charge-mode electrometer measurements of S-isotopic compositions on SHRIMP-SI

T.R. Ireland*, N. Schram, P. Holden, P. Lanc, J. Ávila, R. Armstrong, Y. Amelin, A. Latimore, D. Corrigan, S. Clement, J.J. Foster, W. Compston

Research School of Earth Sciences, The Australian National University, Canberra ACT 0200, Australia

ARTICLE INFO

Article history:
Received 17 September 2013
Accepted 20 December 2013
Available online 9 January 2014

Keywords:
Electrometer measurements
Charge mode
Ion microprobe
Detection systems
Isotope ratio measurement

ABSTRACT

Measurement of ion currents is fundamental to isotope ratio measurements. For small signals, discrete ion arrivals can be detected in pulse counting systems. This procedure works well until a few hundred thousand counts per second when dead time and gain drift become significant. Where sufficiently high signal is available, ion currents can be measured directly in Faraday cups coupled to electrometers with high ohmic (10^{11}, 10^{12} Ω) resistors. However, electrometers measuring current are limited by Nyquist–Johnson noise inherent in the high ohmic resistors to effective count rates above 500,000 c/s. Electrometers can also be operated in charge mode where the feedback resistor is replaced by a capacitor. In this method, charge can be accumulated on the capacitor and the ion current determined by the change in voltage with time. We have implemented this system on the secondary ion mass spectrometer SHRIMP-SI and demonstrate its performance in comparison to the electron-multiplier pulse-counting system and the current mode of the electrometers for S isotope measurements. Of particular interest to us is the measurement of the low abundance ^{36}S isotope (0.015%). From pyrite samples, we have performed 4-isotope analyses with the initial $^{36}S^-$ count rate of 100,000 c/s for a total acquisition time of 720 s. For analyses of mass-fractionation-corrected $^{36}S/^{32}S$ ratios on S isotope standards Ruttan and Balmat, we obtain standard deviations of the measurements of 0.21 and 0.27‰, and standard errors of the means of 0.07 and 0.13‰, respectively. These measurements demonstrate that charge mode can extend the range of electrometer measurements to allow isotope ratio determinations at the 0.1‰ level from signals of 100,000 c/s. Charge mode offers a fast, responsive system, with little gain drift, and is ideally suited to in situ analysis on an ion microprobe.

1. Introduction

An isotope measurement requires the determination of the relative signal strengths of ion beams arriving at a detector or detectors. An ion beam consists of a stream of charged particles and two fundamental means of measuring signal strength are commonly used. Electrometer measurements have generally treated the arrival of the ions as a current, hence *current* mode, where the ion signal measurement is based on the current flow through a high-ohmic resistor in a negative feedback loop on a high-gain amplifier (Fig. 1). This is well suited to ion beams with relatively high signal strengths, of order of 10^{-13} A or higher (order 10^6 c/s), because of the limits imposed at low signal strengths by Nyquist–Johnson noise produced by thermal electrons in the circuit.

Nyquist–Johnson noise has the characteristic of a current source with magnitude according to the well known relationship

$$\Delta I^2 = 4kt\frac{\Delta f}{R} \quad \text{or} \quad \Delta V^2 = 4kT\Delta fR$$

where ΔI is the noise current (rms), ΔV is the noise voltage (rms), k is Boltzmann constant, T is the absolute temperature, R is the feedback resistance, and Δf is the frequency bandwidth of the system. Effectively Nyquist–Johnson noise provides the minimum background current noise for a resistive circuit. For a 10^{11} Ω resistor, operating at room temperature, and a bandpass of 1 Hz, this corresponds to a current of 4×10^{-16} A (rms), or a voltage of 40 μV (rms). In terms of peak-to-peak noise, this corresponds to a current of 2×10^{-15} A, or a count rate of about 12,500 c/s for a peak-to-peak/rms ratio of 5:1 for a random noise voltage [1].

Abbreviations: CDEM, continuous dynode electron multiplier; DDEM, discrete dynode electron multiplier; ESA, electrostatic analyzer; ICP-MS, inductively coupled plasma mass spectrometry; MSWD, mean square of weighted deviates; SHRIMP-SI, sensitive high resolution ion microprobe – stable isotope; SIMS, secondary ion mass spectrometry; TIMS, thermal ionization mass spectrometry.

* Corresponding author at: Research School of Earth Sciences, Building 142, Mills Rd, The Australian National University, Canberra ACT 0200, Australia.
Tel.: +61 2 61255172.
E-mail address: trevor.ireland@anu.edu.au (T.R. Ireland).

1387-3806/$ – see front matter © 2014 Elsevier B.V. All rights reserved.
http://dx.doi.org/10.1016/j.ijms.2013.12.020

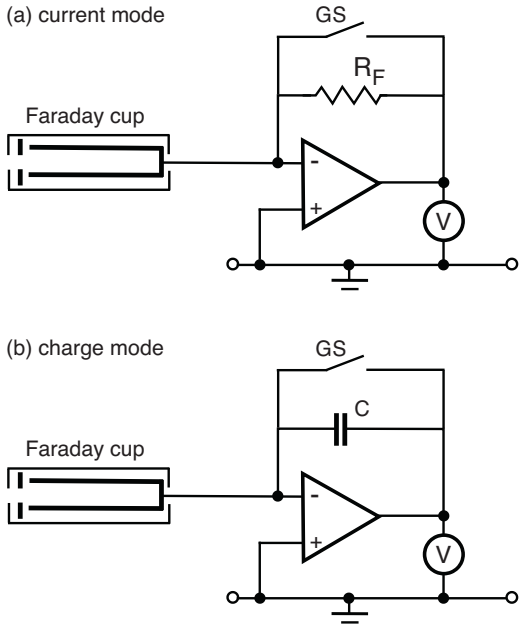

Fig. 1. Electrometer configurations. Schematic circuit diagram of detection system showing configurations used for current mode and charge mode. Both are negative feedback amplifier configurations wherein the high gain amplifier maintains the (−) terminal at the same potential as the (+) terminal, in this case at "virtual ground" potential. (a) In current mode, incoming ions to the Faraday cup cause a change in voltage at (−) terminal. The amplifier acts to maintain ground potential by putting out current to flow back through the feedback resistor R_F. This output can be continuously read through the voltmeter. (b) In charge mode, ions coming in to the Faraday cup cause charge to be stored on the capacitor C. The amplifier responds by putting out a current that changes according to the accumulation of charge. The ion signal can be determined therefore by the rate of change of voltage on the voltmeter. After an analysis, the capacitor can be discharged by closing the ground switch (GS).

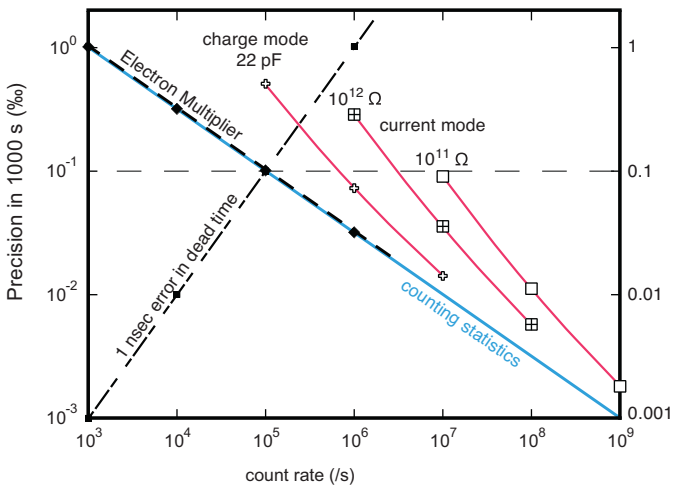

Fig. 2. Theoretical precisions attainable for different detector systems. Illustrated is precision achievable with 1000 s integration time. The ion beam can be regarded as the arrival of discrete charge carriers and so the fundamental limit on precision is governed by counting statistics ($s = 1/\sqrt{N}$, where N is the number of counts). Pulse counting through an electron multiplier is generally regarded as being limited by counting statistics, but accuracy of the dead time correction becomes an issue for high count rates. In the example shown, the dead time has been adjusted by 1 ns (from 20 ns to 19 ns) and the deviation expressed in permil. A 1 ns dead time error becomes an important contributor to uncertainty at count rates above 100,000 c/s yielding a systematic bias to a ratio measurement. Faraday cup measurements using high ohmic resistors (10^{11} Ω, 10^{12} Ω) effectively treat the ion beam as a current source (*current* mode) with a voltage read back across the resistor (Fig. 1a). Their precision is limited by the contribution to the signal of Nyquist–Johnson noise. In charge mode (Fig. 1b), the resistor is replaced by a capacitor which allows charge to build up for a specified integration time before the voltage is read. In this case the noise is limited by thermal noise. Charge mode offers a bridge between Faraday Cup measurements where Nyquist–Johnson noise becomes a limit, and electron multipliers, where gain drift (effectively changing the dead time) starts to become an issue at 10^5 c/s for measurements striving to achieve 0.1‰ precision. Figure adapted from [22].

The lower range of current–mode voltage measurements can be extended by using higher ohmic resistors such as 10^{12} Ω or even 10^{13} Ω [2]. However, these resistors have increasing drawbacks particularly with the longer time constant of the circuit, with settling times being of the order of seconds. While this is not a particular limitation for isotope measurements performed on homogenized samples such as prepared for noble-gas mass spectrometry, thermal ionization mass spectrometry (TIMS), or solution-based inductively coupled-plasma mass spectrometry (ICP-MS) measurements, application to in situ analysis can be more problematical. In situ analysis is performed by ablation of the target either by particle (ion-beam) in secondary ion mass spectrometry (SIMS), or photon (pulsed laser) in laser ablation ICP-MS. In these techniques, rapid changes in ion intensity are common and so use of resistors of high ohmic value and long time constant could induce instrumental artifacts in the data.

Discrete arrivals can be detected with pulse-counting systems utilizing an electron multiplier to generate sufficient signal for detection above background noise. Electron multipliers typically have very low noise floors, of order 0.01 counts per second, making them ideal for very low count-rate measurements. However, electron multipliers have an associated dead time when the device has been triggered, and this, along with the uncertainty in the dead time and the maximum current that can be drawn from the multiplier, places a restriction on the maximum count rate that can be measured to a specified level of uncertainty [3]. The count rate where dead time issues begin to have a significant impact is around 10^5 c/s (for dead time of order of 20 ns). Thus, between the lower level of electrometer measurements at 10^6 c/s and the upper level of pulse counting systems at 10^5 c/s is a gray area where neither technique can achieve performance better than around the 1‰ level (Fig. 2).

An alternative to *current*-mode detection with the electrometer is *charge* mode. In this configuration of the electrometer, the resistor is replaced by a capacitor. Charge from the ion beam is accumulated on the capacitor, with the negative feedback loop being driven by the rate of change of the voltage on the amplifier output. This method has immediate benefit in effectively eliminating the Johnson Noise of the circuit. But there are additional benefits in effectively instantaneous settling time, the ability to integrate the signal over a specified time period, and minimizing noise associated with the shunt capacitance, particularly the noise gain associated with the input capacitance relative to the feedback capacitance [1]. Thermal noise (rms) for a capacitor [4] can be expressed as

$$\Delta V^2 = \frac{kT}{C}$$

For a 10 pF capacitor, this corresponds to a noise voltage of 20 μV, only a factor of 2 less noise than a 10^{11} Ω resistor. However, this noise is not inherent to the capacitor, but rather the statistical equilibrium of the charge in the capacitor. As such, the noise is apparent only for the reading of the capacitor and the effects can be minimized by selection of an appropriately long integration time during data acquisition.

The use of a capacitor as the feedback element in an electrometer head was a standard inclusion in Cary electrometers that were widely used for mass spectrometric measurements until the 1980s when solid state electrometers became more fashionable. The facility was rarely utilized, probably due to limited computational flexibility of the period. At face value, charge mode offers lower noise and effectively immediate response times. However,

there are issues; maintaining a constant, low capacitative coupling in a collector has proven to be difficult [5]. Further, in measuring the voltage in the charge mode configuration, additional noise can be introduced during switching, and measurement error can be a significant component for low differential signals.

One of our recent goals has been to optimize the detection system of our SHRIMP-SI (Sensitive High Resolution Ion Microprobe for Stable Isotopes) for measurement of sulfur isotopes. Analysis of sulfur isotopes is a good test of a detector system because of the large differences in isotopic abundances with ^{32}S 95.04%, ^{33}S 0.75%, ^{34}S 4.20%, and ^{36}S 0.015% [6]. Measurement of ^{32}S–^{33}S–^{34}S in sulfides on an ion microprobe can be carried out with Faraday cups and current-mode electrometers utilizing 10^{11} or 10^{12} resistors. Effective count rates of $^{33}S^-$ up to 30 MHz can be generated, and subpermil precision is readily achievable [7,8]. However, the measurement of low-abundance ^{36}S is becoming increasingly important in geochemistry to resolve differences between Archean photochemical fractionation from biologic fractionations. For measurement with the count rates listed above, the ^{36}S count rate is 140,000 c/s. This places it squarely in the gray area between detection systems: where ion counter measurements begin to require significant dead time and drift corrections, and below the normal lower limit for current-mode Faraday cup measurement. It would be of great practical benefit if Faraday cup measurements could be extended to lower count rates.

Here we describe an implementation of a charge-mode electrometer system on the SHRIMP-SI. We demonstrate that it does fulfill much of the theoretical promise of measuring lower count rates and bridges the gap between current-mode Faraday cup measurements and electron multipliers.

2. Analytical

2.1. SHRIMP-SI

SHRIMP-SI is a secondary ion mass spectrometer configured as an ion microprobe [9]. The primary ion beam for SHRIMP SI is Cs^+ that can be focused from ca. 1 μm up to 30 μm on to polished surfaces. The Cs-ion source is a Kimball Physics model IGS-4 with Cs zeolite as the emitter; Cs ions are initially focused through an accelerating potential of 5 kV. On SHRIMP SI, the sample potential is held at ca. −10 kV resulting in a total primary ion impact energy of 15 keV at the target. An electron gun, grounded at the sample potential, can be used to introduce electrons to the target for charge neutralization at an incident energy of ca. 1.5 kV. Negative secondary ions are accelerated to real ground from the −10 kV sample potential and beam transmission is maximized to the source slit with an einzel lens system after the acceleration gap and a quadrupole triplet lens system similar to that used on other SHRIMP models [9]. SHRIMP-SI uses the same forward-geometry as SHRIMP-II instruments with a double-focusing mass analyzer design [10] to enable high mass resolution ($5000M/\Delta M$ at 1% peak width for 100 μm entrance and exit slits) while maintaining high sensitivity through a physically large mass spectrometer (magnet turning radius of 1000 mm).

The original design of SHRIMP-SI included a multiple collector with one axial fixed head, and two floating heads for low mass and high mass (relative to axial). The detector heads on the axial and floating heads are mounted on solid lead-throughs; detector housings allow the complete containment of a Faraday cup or a large ETP^{TM} electron multiplier (model AF150H). The external electrometer housing and lead through are evacuated to roughing vacuum,

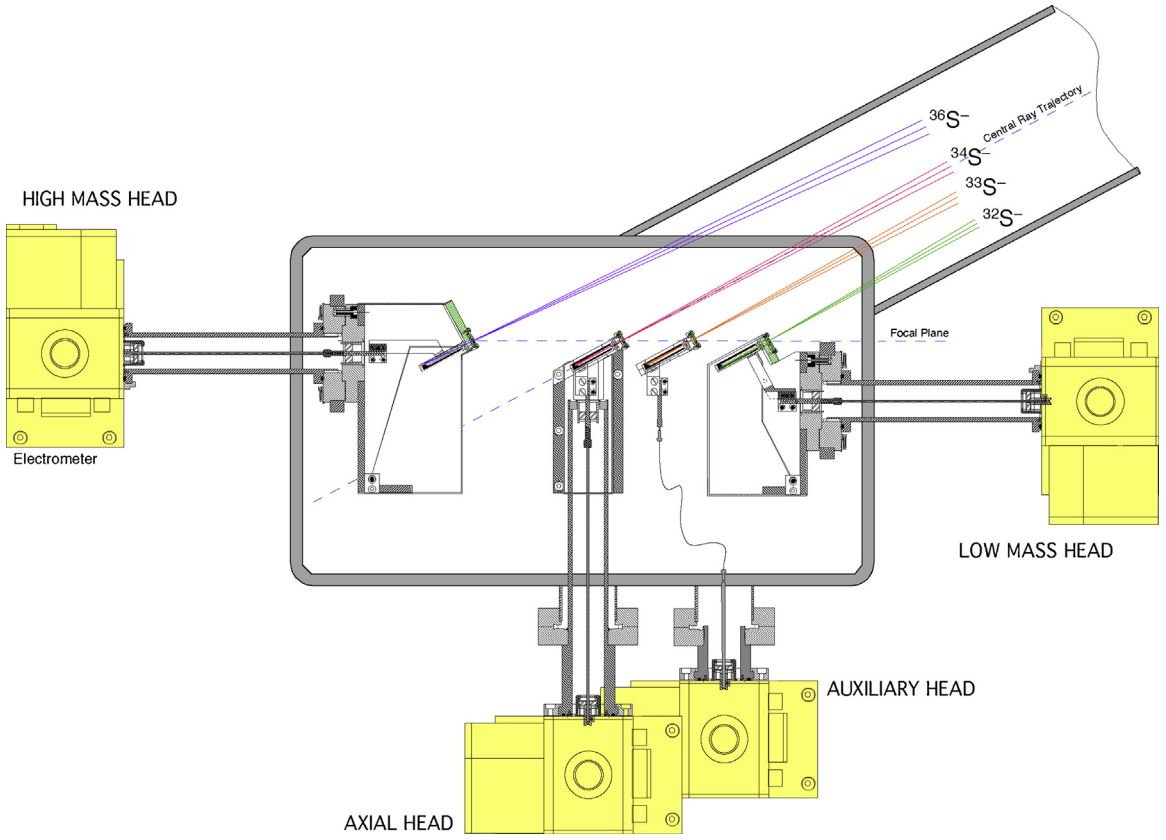

Fig. 3. SHRIMP SI multiple collector configuration. The original multiple collector consisted of three collectors with solid lead throughs to facilitate charge mode collection. These three collector heads can also house ion counters. The multiple collector has been reconfigured with an additional auxiliary head, with a flexible coupling link, to allow the collection of ^{33}S in current mode. Shown is the configuration used for 4-isotope sulfur analysis.

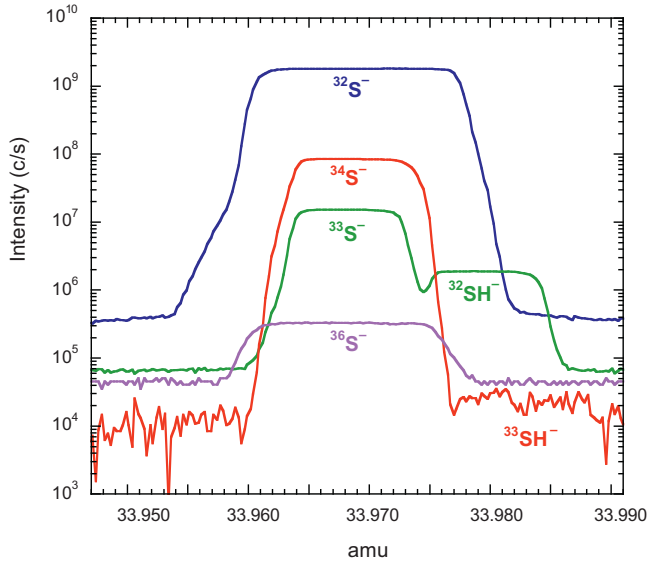

Fig. 4. Mass spectra of the sulfur mass region. X-axis is determined by the ^{34}S mass position and is applicable to mass-34 only. Collector slit widths used: ^{32}S = 400 μm, ^{33}S = 150 μm, ^{34}S = 200 μm, ^{36}S = 300 μm. Signals collected on: ^{32}S (10^{11} Ω resistor), ^{33}S and ^{34}S (10^{12} Ω resistor), ^{36}S (22 pF capacitor). The only interferences observed were sulfur hydrides at mass 33 and mass 34. With the appropriate collector slit widths, the hydride peaks are well resolved.

with a vacuum break to the high vacuum of the collector chamber (2×10^{-8} mbar) provided by a sapphire insert.

Electrometer and electron multiplier signals are independently exported to the Digital Acquisition System. In order not to compromise either detection system, it was decided that each detector head would involve either an electron multiplier or a Faraday cup for an analytical session, with interchange between the two requiring the multi-collector to be vented, the detectors changed, and the collector then re-evacuated.

During the course of this work the multiple collector was reconfigured with a fourth detector added that would allow sulfur 4-isotope measurements (Fig. 3). This fourth detector is fixed in position and connected to the electrometer with a flexible coaxial cable.

2.2. Mass spectrometry

For the S isotope measurements presented here a 60 μm source slit was used. The collector slit widths were set at 400 μm for $^{32}S^-$, 150 μm for $^{33}S^-$ (to resolve $^{32}SH^-$), 200 μm for $^{34}S^-$, and 400 μm for $^{36}S^-$. The only interferences we noted were those of sulfur hydrides (Fig. 4) at mass 33 ($M/\Delta M$ of 4000 required) and mass 34 ($M/\Delta M$ of 3000) with $^{33}SH^-$ only barely resolvable above background.

SHRIMP-SI features a novel steering system built in to the first extraction plate above the target surface. This system allows steering into the secondary extraction column so that the beam trajectory can be controlled from the outset of beam focusing and allows the beam to be confined to the central ray trajectory. With a 45° primary beam incidence angle, any discrepancy in optical focusing will cause a lateral shift of the primary beam of the same magnitude. The extraction steering allows this discrepancy to be accommodated at the earliest stage of beam transport.

Automated secondary ion tuning involves only steering of the secondary ion beam. The first stage is the *Y* and *Z* steering on the extraction electrode (with *X* being the beam transport direction). This steering is used to steer the secondary ion beam through the differential pumping aperture. The beam is then steered in *Y* and *Z* after the quadrupole triplet through the source slit. Post-source-slit deflection is then used to maximize beam intensity at the collector.

2.3. Ion-counting measurement

In single collector mode, the secondary ion signal measured on an ion counter is accumulated over several cycles through the peak sequence and so any gain drift is effectively normalized out in the data reduction process (e.g. Dodson interpolation [11]). The ultimate accuracy for single ion counter measurements appears to be of the order of 0.3‰ (1σ) under optimal circumstances. For example, for a counting system with a 1 ns uncertainty in the dead time, getting to 0.3‰ precision in the $^{34}S/^{32}S$ ratio requires an optimum $^{32}S^-$ count rate of 180,000 c/s and a minimum time of 3000 s [3]. Even this might be optimistic given the issues with dead time [3], differences in dead time for different elements [12], and the gain drift associated with aging of the multiplier.

Multiple collection by ion counting is far more difficult. Calibration of multiple ion counters can also be carried out through analysis of reference materials so that external corrections can be applied through the analytical session. However, the drift must be calibrated for each individual ion counter and the uncertainties of the standard measurements and drift rates need to be propagated to the targets being measured. The drift rate is strongly correlated with the count rate so different detectors will drift at different rates depending on the species and its count rate.

Our initial multiple ion counting studies were applied to the identification of ancient Archean zircons on SHRIMP-II [13]. Space limitations with the SHRIMP-II multi-collector precluded the use of large discrete-dynode electron multipliers (DDEM) and so Sjuts 408 continuous-dynode electron multipliers (CDEM) were used instead. The performance of the multiple-ion-counting system was adequate for the Pb isotope measurements. However, Si isotope measurements demonstrated significant drift over short periods of time as the gain of two CDEM (for $^{29}Si^+$ and $^{30}Si^+$) changed with respect to the reference Faraday cup measurement of $^{28}Si^+$ even at only moderate count rates (c. 50 kHz). Furthermore, scrutiny of the after-pulse period revealed multiple pulsing for at least 200 ns after the main arrival further compromising their accuracy. Consequently the multiple collector for SHRIMP-SI was designed to use the large ETP DDEM in an attempt to measure signal strengths up to 1 MHz on the premise that drift characteristics would be superior to CDEM. The SHRIMP-SI pulse counting system includes an amplifier/discriminator system with a gated dead time of 30 ns, which is greater than the measured 22 ns dead time.

2.4. Electrometer measurement

In *current* mode, the arrival of the negative secondary ion beam at the input node of the amplifier generates an electron flow back through the feedback resistor to effectively keep the Faraday cup at ground potential. Typically, resistors of 10^{10} or 10^{11} Ω are used to generate a minimum signal of around 50 mV and to a maximum of 50 V for measurement. This equates to currents ranging from 5×10^{-13} to 5×10^{-9} A and effective count rates of 3×10^6–3×10^{10} c/s. At the upper end of this scale, secondary ion emission from typical targets used to generate O^- and S^- beams on SHRIMP-SI are limited to a few GHz and so exceeding the maximum voltage is not really an issue. The lower end of measurable secondary ion signals can be extended with 10^{12} Ω resistors to count rates around the 500,000 c/s level.

Secondary ions are captured in the Faraday cup located behind the collector slit of the detector head. The impact can create secondary electrons and loss of an electron effectively reduces the negative ion count rate that is detected. The secondary electrons are contained through having an electron repeller in front of the

cup with a moderate negative voltage (−90 V). The collector slits are of fixed width (ranging from 100 to 400 μm) and can be manually interchanged. This system has the advantage of ensuring slit alignment with the detector. While a requirement to vent the chamber to change slits is a compromise, in reality only a few collector slit configurations are required for stable isotope work and interchange only happens on an irregular basis.

A new electrometer system has been developed to allow combined current and charge mode. The iFlex electrometer has 10^{10} Ω, 10^{11} Ω, and 10^{12} Ω resistors and a 22 pF capacitor, which are remotely selectable via reed relays. The high live-time *V–F* convertor data acquisition system incorporates a bias current to accommodate bipolar noise signals in the otherwise unipolar system. Output voltages from the iFlex are converted to a pulse train via a 1 MHz V-F converter. Digital resolution of the V-F converter is selected via a programmable gain amplifier allowing 0–50 mV, 0–500 mV, 0–5 V and 0–50 V as full scale. Software converts the measured frequency back to ion current and thence ion-arrivals per second depending on which resistor and which V-F range has been selected.

For charge mode acquisition, the inferred ion current is determined by the rate of change of the voltage at the amplifier output according to

$$i = C\,\frac{dV}{dt}$$

where i is the current, C is the capacitance, and dV/dt the rate of change of the voltage. Implicit in this equation is that the source capacitance of the system is negligible compared to the integration capacitor, and that it remains constant. Hence the Faraday cups are rigidly attached to the iFlex via solid copper rods, thereby minimizing the potential capacitance fluctuation caused by vibration or other geometric change. The feedback ammeter configuration of the iFlex electrometer effectively neutralizes the Faraday cup capacitance by maintaining the input node at 0 V, except for brief transient situations.

During acquisition, the Faraday cup receives charge through the incoming ion beam. The rate of change of the voltage is measured directly and an effective ion current determined. A single acquisition consists of a 20 s integration, which is divided into 10 sub-integrations of 2 s; the firmware in the Digital Acquisition System returning the frequency change related to each 2 s integration to the control computer. The 10 sub "counts" are subjected to a statistical test for outliers before being converted and stored as the equivalent ion-current (as c/s) for the 20 s integration period.

The choice of the V-F range from which the voltage change is calculated is crucial. The analyst faces a choice, discharge the capacitor at the end of each acquisition or allow the charge to accumulate over the whole period of the analysis. For the former scenario, a narrow voltage range could be chosen for improved digital resolution in each acquisition, but the discharge causes a disruption to the system as a whole and could cause variability in the starting voltage. In the latter situation, the acquisition can continue uninterrupted for the analysis but at the expense of coarser measurement resolution as the total accumulated voltage increases. For these measurements we have chosen to discharge the capacitor at the beginning of each analysis during the raster period so as to allow sufficient settling time (30 s) before data acquisition.

3. Measurements

3.1. Multiple collector S isotope measurements on SHRIMP SI

The SI multi-collector was initially designed with two moving heads and a fixed axial detector sufficient for the measurement of $^{32}S^-$, $^{33}S^-$, and $^{34}S^-$. In the experiments (i–iv) that are described below this configuration is used. In experiment (v), the positions of the detector heads were moved such that $^{32}S^-$ and $^{36}S^-$ were in the low and high mass detectors respectively. These experiments are designed to allow comparison of performance of current mode and charge-mode operation of the electrometers, and the electron multiplier counting system.

Pyrite was used as the target mineral and so no electron-beam charge neutralization was applied because of the conductivity of the sulfide and the lack of any benefit that could be observed in using it. Sputtering of the pyrite sample begins with rastering the primary beam over an area slightly larger than the spot for 1 min. This removes the gold coat and allows conditioning of the sample surface with Cs. Once the raster is completed the primary ion beam is allowed to sputter the target for a further minute. During the raster and delay period, an in-line valve between sample chamber and ESA is closed and base-lines for the electrometers are collected. Data collected from spot measurements consisted of 4 sets of 20 s (i.e. 80 s total), with each set consisting of ten 2 s integrations.

Data are expressed in delta notation such that ratios are expressed as permil deviations from a reference value, e.g.

$$\delta^{34}S = \left[\frac{(^{34}S/^{32}S)_{measured}}{(^{34}S/^{32}S)_{reference}} - 1\right] \times 1000$$

where $(^{34}S/^{32}S)_{measured}$ is the measured $^{34}S^-/^{32}S^-$ ratio, $(^{34}S/^{32}S)_{reference}$ is the reference value of that ratio used for normalization, and $\delta^{34}S$ is expressed in permil (‰) deviation. A similar formulation is used for $\delta^{33}S$ and $\delta^{36}S$.

3.2. Experiment (i)

[^{32}S on 10^{11} Ω, ^{33}S on electron multiplier, ^{34}S on 10^{12} Ω; $^{32}S^-$ count rate 43 MHz.]

The S^- beam intensity was adjusted so that the $^{33}S^-$ could be measured on the electron multiplier of the axial detector at 300,000 c/s. This was viewed as an appropriate test of the ion counting system based around the ETP multipliers. The multipliers commonly run with count rates at this level in U–Pb geochronology albeit for short periods on high intensity species such as UO^+ and ThO^+. $^{32}S^-$ and $^{34}S^-$ were measured on electrometers in current mode with feedback resistors of 10^{11} Ω (50 V range) and 10^{12} Ω (5 V range) respectively with effective count rates of 50 MHz and 2.2 MHz respectively. Ten replicate spots were measured. Data are presented in Table 1 Expt (i).

The $^{34}S^-/^{32}S^-$ shows excellent reproducibility in this experiment (Fig. 5(a)). Normalized to the mean of the $^{34}S/^{32}S$ ratios, $\delta^{34}S$ shows a total variation from −0.18 to +0.50‰ with a standard deviation of 0.21‰ and standard error of 0.07‰. A weighted mean of all analyses has an MSWD of 3.3 indicating the data are overdispersed compared to their internal measurement errors. One value is removed from the overall distribution and is likely an outlier with it being 4.5 sigma above the mean. If this analysis is rejected then the weighted mean is -0.04 ± 0.03‰ (1σ) with an MSWD of 0.93. This data therefore indicates that the individual internal errors of an analysis can be consistent with the distribution of the data for an analytical session.

However, this performance is not replicated in the $^{33}S/^{32}S$ results. The $\delta^{33}S$ data are normalized to the first analysis of the session and show a systematic fall of nearly 50‰ over the course of the ten analyses in the session (Fig. 5(b)). This is entirely due to the downward drift in the relative gain of the axial ETP multiplier used for the $^{33}S^-$ measurement. During the analysis the signal intensity of $^{33}S^-$ falls and is only recoverable by raising the gain of the multiplier by increasing the applied voltage across the dynode chain. Thus even at 300,000 c/s, substantial drift is occurring on the

Table 1
Sulfur isotope ratio measurement experiments.

Expt (i)	Electrometer (R11)* – electron multiplier – electrometer (R12)							
Species	^{32}S	^{33}S	^{34}S					
Count rate	43 MHz	0.3 MHz	1.9 MHz					
	$^{33}S/^{32}S$	Error	$\delta^{33}S$ (‰)[a]	Error (‰)	$^{34}S/^{32}S$	Error	$\delta^{34}S$ (‰)[b]	Error
1	0.006829	1.3658E−06	0.0	0.20	0.043792	0.0000044	−0.14	0.10
2	0.00678	0.0000040680	−7.2	0.60	0.043820	0.0000048	0.50	0.11
3	0.006742	2.6968E−06	−12.7	0.40	0.043790	0.0000074	−0.18	0.17
4	0.006731	2.6924E−06	−14.4	0.40	0.043800	0.0000035	0.04	0.08
5	0.006677	0.0000016693	−22.3	0.25	0.043797	0.0000039	−0.03	0.09
6	0.006658	3.9948E−06	−25.0	0.60	0.043802	0.0000053	0.09	0.12
7	0.006608	0.0000020485	−32.4	0.31	0.043793	0.0000044	−0.12	0.10
8	0.006556	0.0000021635	−40.0	0.33	0.043803	0.0000053	0.11	0.12
9	0.006511	0.0000023440	−46.6	0.36	0.043790	0.0000057	−0.18	0.13
10	0.006491	1.9473E−06	−49.5	0.30	0.043794	0.0000039	−0.09	0.09
Mean	0.006658		−25.0		0.043798		0.00	
Std dev	0.000115		16.9		0.000009		0.21	
Std err	0.000038		5.6		0.000003		0.07	

Expt (ii)	Electrometer (R11) – electron multiplier – electrometer (R12)							
Species	^{32}S	^{33}S	^{34}S					
Count rate	7 MHz	0.05 MHz	0.3 MHz					
	$^{33}S/^{32}S$	Error (σ)	$\delta^{33}S$ (‰)[c]	Error (σ)	$^{34}S/^{32}S$	Error (σ)	$\delta^{34}S$ (‰)[b]	Error (σ)
1	0.00685	0.000004453	2.25	0.65	0.043595	0.0000131	1.00	0.30
2	0.006864	0.000003432	4.30	0.50	0.04353	0.0000131	−0.49	0.30
3	0.00685	0.000003425	2.25	0.50	0.043517	0.0000148	−0.79	0.34
4	0.006813	0.000002725	−3.24	0.40	0.043543	0.0000113	−0.19	0.26
5	0.006833	0.000002050	−0.24	0.30	0.043522	0.0000196	−0.68	0.45
6	0.006856	0.000004799	3.13	0.70	0.043525	0.0000135	−0.61	0.31
7	0.006801	0.000005441	−4.92	0.80	0.043594	0.0000218	0.98	0.50
8	0.006827	0.000008465	−1.11	1.24	0.043573	0.0000161	0.49	0.37
9	0.006818	0.000004773	−2.43	0.70	0.043564	0.0000218	0.29	0.50
Mean	0.006835		0.00		0.043551		0	
Std dev (σ)	0.000022		3.16		0.000031		0.71	
Std err (σ)	0.000008		1.12		0.000011		0.25	

Expt (iii)	Electrometer (R11) – electron multiplier – electrometer (R11)							
Species	^{32}S	^{33}S	^{34}S					
Count rate	7 MHz	0.05 MHz	0.3 MHz					
	$^{33}S/^{32}S$	Error (σ)	$\delta^{33}S$ (‰)[c]	Error (σ)	$^{34}S/^{32}S$	Error (σ)	$\delta^{34}S$ (‰)[b]	Error (σ)
1	0.006756	0.000002500	−5.17	0.37	0.040361	0.000054	−3.04	1.35
2	0.0068	0.000004352	1.31	0.64	0.040496	0.000075	0.30	1.86
3	0.006813	0.000002589	3.22	0.38	0.040508	0.000047	0.59	1.16
4	0.006803	0.000004490	1.75	0.66	0.040447	0.000041	−0.91	1.01
5	0.006798	0.000004691	1.01	0.69	0.040555	0.000059	1.75	1.45
6	0.0068	0.000003468	1.31	0.51	0.040560	0.000066	1.88	1.62
7	0.00678	0.000004068	−1.64	0.60	0.040432	0.000051	−1.28	1.27
8	0.00678	0.000002034	−1.64	0.30	0.040509	0.000061	0.62	1.5
9	0.00679	0.000004074	−0.16	0.60	0.040488	0.000059	0.10	1.46
Mean	0.006791		0.00		0.040484		0	
Std dev (σ)	0.000017		2.50		0.000063		1.55	
Std err (σ)	0.000006		0.88		0.000022		0.55	

Expt (iv)	Electrometer (R11) – electron multiplier – electrometer (C)							
Species	^{32}S	^{33}S	^{34}S					
Count rate	7 MHz	0.05 MHz	0.3 MHz					
	$^{33}S/^{32}S$	Error (σ)	$\delta^{33}S$ (‰)[c]	Error (σ)	$^{34}S/^{32}S$	Error (σ)	$\delta^{34}S$ (‰)[b]	Error (σ)
1	0.006808	6.4676E−06	1.60	0.95	0.041127	0.000011	−0.34	0.26
2	0.006799	5.50719E−06	0.28	0.81	0.04113	0.000006	−0.27	0.15
3	0.006813	2.0439E−06	2.34	0.30	0.041133	0.000013	−0.20	0.32
4	0.006787	3.05415E−06	−1.48	0.45	0.041132	0.000015	−0.22	0.36
5	0.006804	2.7216E−06	1.02	0.40	0.041154	0.000010	0.31	0.25
6	0.006783	1.96707E−06	−2.07	0.29	0.041148	0.000007	0.17	0.18
7	0.006791	5.36489E−06	−0.90	0.79	0.041161	0.000003	0.48	0.07
8	0.006795	5.5719E−06	−0.31	0.82	0.04114	0.000006	−0.03	0.15
9	0.0068	0.00000442	0.43	0.65	0.041165	0.000014	0.58	0.34
10	0.006797	2.44692E−06	−0.01	0.36	0.041137	0.000008	−0.10	0.19

Table 1 (*Continued*).

Expt (iv)	Electrometer (R11) – electron multiplier – electrometer (C)							
Species	^{32}S	^{33}S	^{34}S					
Count rate	7 MHz	0.05 MHz	0.3 MHz					
	$^{33}S/^{32}S$	Error (σ)	$\delta^{33}S$ (‰)[c]	Error (σ)	$^{34}S/^{32}S$	Error (σ)	$\delta^{34}S$ (‰)[b]	Error (σ)
11	0.006791	3.59923E−06	−0.90	0.53	0.041126	0.000007	−0.37	0.16
Mean	0.006797		0.00		0.041141		0	
Std dev (σ)	0.000009		1.32		0.000014		0.33	
Std err (σ)	0.000003		0.42		0.000004		0.11	

Expt (v)	Electrometer (R11) – electrometer (C)			
Species	^{32}S	^{36}S		
	700 MHz	0.1 MHz		
	$^{36}S/^{32}S$	Error (σ)	$\delta^{36}S$ (‰)[d]	Error (σ)
1	0.00014077	0.00000004	−0.86	0.31
2	0.00014086	0.00000004	−0.22	0.28
3	0.00014094	0.00000005	0.35	0.35
4	0.00014091	0.00000002	0.14	0.17
5	0.00014087	0.00000006	−0.15	0.44
6	0.00014092	0.00000006	0.21	0.4
7	0.00014078	0.00000005	−0.78	0.36
8	0.00014096	0.00000006	0.49	0.4
9	0.00014091	0.00000006	0.14	0.45
10	0.00014098	0.00000004	0.63	0.29
11	0.00014101	0.00000003	0.85	0.22
12	0.00014102	0.00000006	0.92	0.41
13	0.00014087	0.00000003	−0.15	0.18
14	0.0001408	0.00000005	−0.64	0.38
15	0.00014083	0.00000004	−0.43	0.3
16	0.00014087	0.00000004	−0.15	0.31
17	0.00014084	0.00000004	−0.36	0.29
Mean	0.00014089		0	
Std dev (σ)	0.00000008		0.53	
Std err (σ)	0.00000002		0.13	

Note: R11 refers to use of a 10^{11} Ω feedback resistor on the electrometer.
R12 refers to use of a 10^{12} Ω feedback resistor on the electrometer.
C refers to use of a 22 pF capacitor on the electrometer.
Analytical analyses are expressed at 1σ level.
[a] $\delta^{33}S$ normalized to first $^{33}S/^{32}S$ analysis.
[b] $\delta^{34}S$ normalized to mean of $^{34}S/^{32}S$ analyses.
[c] $\delta^{33}S$ normalized to mean of $^{33}S/^{32}S$ analyses.
[d] $\delta^{36}S$ normalized to mean of $^{36}S/^{32}S$ analyses.

multiplier. This is a disappointingly similar result to the Si isotope drifts observed for the Sjuts CDEM [13].

3.3. Experiment (ii)

[$^{32}S^-$ on 10^{11} Ω, $^{33}S^-$ on electron multiplier, $^{34}S^-$ on 10^{12} Ω; $^{32}S^-$ count rate 7 MHz.]

The second configuration involves reducing the count rate on $^{33}S^-$ in an attempt to stabilize the electron multiplier. The experiment was repeated at a $^{33}S^-$ count rate of 50,000 c/s (0.3 MHz $^{34}S^-$ and 7 MHz $^{32}S^-$) with the same collector configuration. $^{32}S^-$ and $^{34}S^-$ were measured by current mode with resistors of 10^{11} Ω (5 V range) and 10^{12} Ω (500 mV) range respectively.

With the reduced beam intensity on the electrometers measuring ^{34}S and ^{32}S, the internal precision falls by a factor of three as would be expected for the lower beam intensity (Fig. 5(c)). Normalized to the mean of the $^{34}S^-/^{32}S^-$ for the session, the $\delta^{34}S$ shows a standard deviation of 0.71‰ with a standard error of 0.25‰. The weighted mean of these analyses is -0.07 ± 0.11‰ (1σ) with an MSWD of 3.9. However there is no clear outlier in this data set suggesting that there may be other noise components that become apparent as the beam size falls.

Although measuring a factor of 6 smaller beam intensity, the statistics for the $^{33}S/^{32}S$ improve significantly (Fig. 5 (d)). Excluding the first analysis, there is a slight downward drift in the data, but the data are quite scattered. The mean $\delta^{33}S$ is −2.3‰ with a standard deviation of 3.2‰ and standard error of 1.1‰. The weighted mean of the analyses has an MSWD of over 30 indicating the measurement errors are not consistent with the data distribution. The internal errors are generally around 0.5‰ as expected from the accumulated counts, but the data are not replicating at this level.

3.4. Experiment (iii)

[$^{32}S^-$ on 10^{11} Ω, $^{33}S^-$ on electron multiplier, $^{34}S^-$ on 10^{11} Ω; $^{32}S^-$ count rate 7 MHz.]

The resistor on the high mass head (measuring $^{34}S^-$) was then switched to a 10^{11} Ω resistor (500 mV range). The purpose of this experiment was to examine the background correction and operation of the V-F conversion system at low effective currents. As expected there is a systematic rise in the uncertainties of the individual $\delta^{34}S$ analyses to over 1‰. The data show a standard deviation of 1.55‰ and standard error of 0.55‰. The weighted mean of the $\delta^{34}S$ values is -0.19 ± 0.45‰ with an MSWD of 1.25 indicating a good correspondence of measurement errors and data distribution (Fig. 5(e)). The $\delta^{33}S$ values for this experiment show a similar degree of scatter to Expt (ii) with a standard deviation of 3.2‰ (Fig. 5(f)) and the data are again overdispersed relative to the measurement errors with an MSWD of 39.

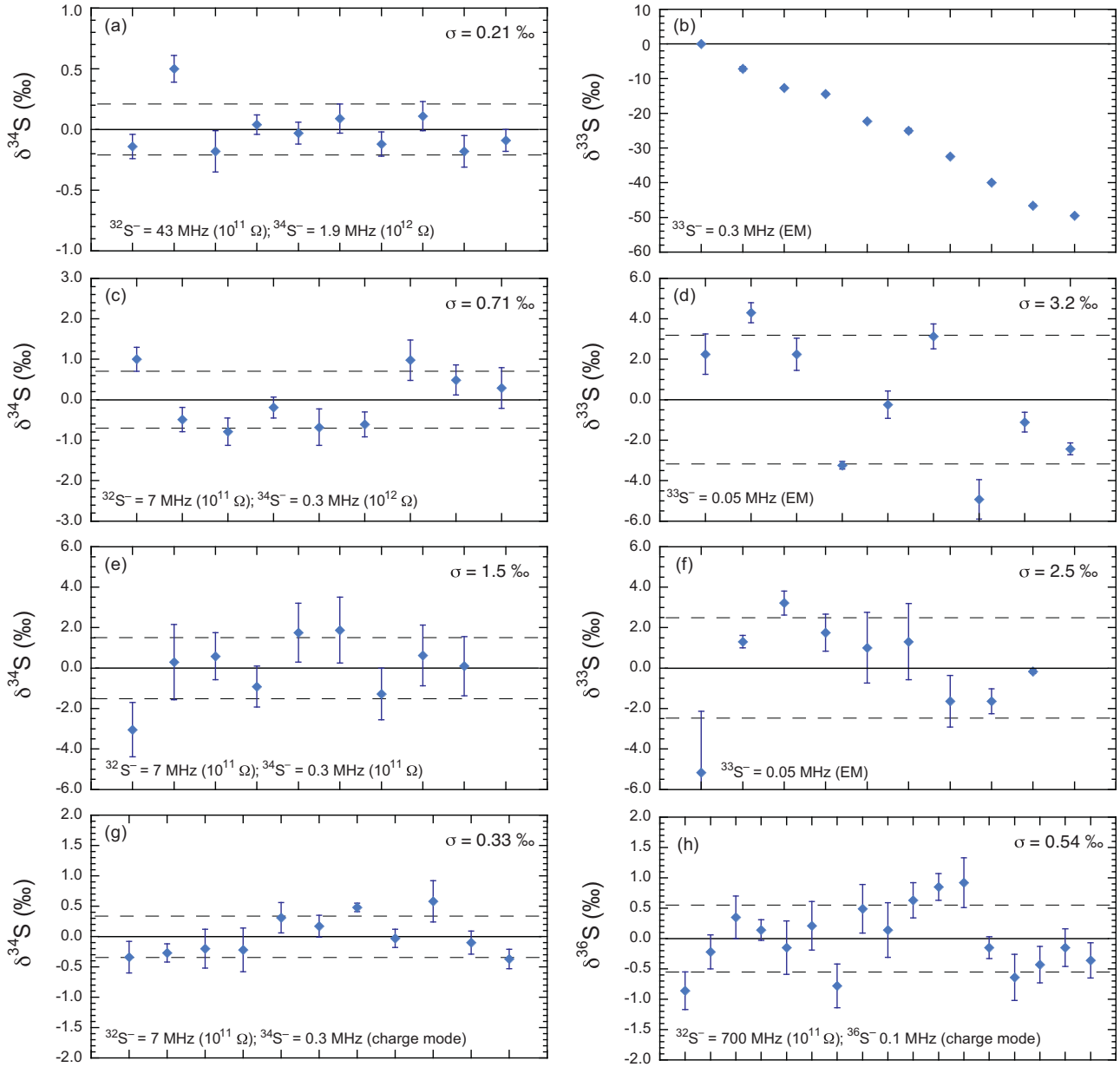

Fig. 5. Sulfur isotope ratios in various detector configurations. (a) ^{32}S measured across 10^{11} Ω resistor, ^{34}S on 10^{12} Ω resistor. $\delta^{34}S$ measured in ten successive measurements and normalized to the mean of the $^{34}S/^{32}S$ values. The standard deviation (σ) of the measurements is 0.21%. (b) ^{33}S measured on electron multiplier at ca. 300,000 c/s [with data from (a)]. $\delta^{33}S$ normalized to the first $^{33}S/^{32}S$ measurement. The $\delta^{33}S$ values show a progressive fall of ca. 50‰ during the course of the data acquisition. This fall is due to gain drift on the electron multiplier. (c) Same configuration as (a and b) with the signal intensity reduced to $^{33}S^-$ count rate of 50,000 c/s. $\delta^{34}S$ normalized to the mean of the $^{34}S/^{32}S$ values. With the lower signal intensity, the standard deviation (σ) of the measurements has increased, relative to (a), to 0.71%. (d) ^{33}S measured on electron multiplier at ca. 50,000 c/s [with data from (c)]. The $\delta^{33}S$ values show a lower drop during the analyses, which is consistent with the change in ratio in (b) being associated with the gain drift during the course of the analyses. The standard deviation of the $\delta^{33}S$ analyses is improved to 3.2‰ but remains high compared to the counting statistics. (e) Same count rates as (c and d) but the electrometer on the $^{34}S^-$ head has been switched to the 10^{11} Ω resistor to assess the V-F converter at low signal strength. The standard deviation of the $\delta^{34}S$ measurements is 1.5‰. (f) $\delta^{33}S$ data analogous to (d). (g) The electrometer on the $^{34}S^-$ head has been switched to charge mode, while maintaining the count rate of $^{32}S^-$ at 7 MHz. The $\delta^{34}S$ data show excellent reproducibility at 0.33‰, which is better than the 10^{12} Ω resistor in current mode (shown in (c)). (h) Detector configuration changed to position $^{32}S^-$ in low mass head and $^{36}S^-$ in high mass head. $^{36}S^-$ measured by charge mode and $^{32}S^-$ by current mode (10^{11} Ω). The data show excellent reproducibility with a standard deviation of all measurements of 0.5‰.

3.5. Experiment (iv)

[$^{32}S^-$ on 10^{11} Ω, $^{33}S^-$ on electron multiplier, $^{34}S^-$ on charge mode; $^{32}S^-$ count rate 7 MHz.]

In this experiment, the iFlex resistor of the high-mass-head electrometer was replaced with the 22 pF capacitor and the electrometer was operated in charge mode. $^{32}S^-$ was collected with current mode (10^{11} Ω resistor, 5 V range). The $\delta^{34}S$ data (normalized to the mean of the data set) show a very tight distribution with a standard deviation of 0.33‰ and standard error of 0.11‰ (Fig. 5(g)). In comparison, the weighted mean is 0.17 ± 0.05‰ but shows excess scatter with an MSWD of 5.2. One analysis (#7 at $+0.48 \pm 0.07$) is high and with very high precision and this is the main contributor to the elevated MSWD. Removing this analysis yields a weighted mean of -0.10 ± 0.06 (1σ) with an MSWD of 1.59. The performance of charge mode is therefore highly encouraging. There is no analytical drift, and the data distribution with standard deviation of 0.3‰ (including analysis #7) is better than either the

10^{11} or 10^{12} Ω resistors in current mode at this signal intensity. During this experiment, the $\delta^{33}S$ values were again scattered with a standard deviation of 2.5‰ and a weighted mean MSWD of 14.

3.6. Experiment (v)

[$^{32}S^-$ on 10^{11} Ω, $^{36}S^-$ on charge mode; $^{32}S^-$ count rate 700 MHz.]

The final configuration tested with the three head collector involved moving the high and low mass heads to accept $^{32}S^-$ and $^{36}S^-$. The axial detector still had the electron multiplier in position but this was not operated owing to the excessively high $^{34}S^-$ count rate that the multiplier would have to accept. As such only the $^{36}S/^{32}S$ and $\delta^{36}S$ (normalized to the mean) are reported in Table 1 Expt (v). The $^{36}S^-$ count rate was set to 100,000 c/s and the corresponding count rate for $^{32}S^-$ was 700 MHz. These are similar count rates to those expected to be used for a full 4-isotope sulfur analysis.

The data are well distributed with a standard deviation of 17 analyses of 0.54‰ and a standard error of 0.13‰ (Fig. 5(g)). The weighted mean of the 17 analyses is 0.02 ± 0.07‰ (1σ) with an MSWD of 3.0. One analysis appears significantly high (3.8σ removed from mean). Removing this analysis (#11) results in a weighted mean of -0.07 ± 0.07‰ and an MSWD of 2.2.

3.6.1. Four-isotope sulfur measurements on SHRIMP SI

In the four detector system (Fig. 3), the fourth auxiliary detector is located at a fixed collector position. It was placed at the requisite distance on the low mass side of the axial position to collect $^{33}S^-$. The two floating heads were used to collect ^{32}S and ^{36}S, with ^{34}S in the axial collector. In these experiments, the four collectors allow the measurement of the four sulfur isotopes that can be expressed as three sulfur isotope ratios $^{33}S/^{32}S$, $^{34}S/^{32}S$, and $^{36}S/^{32}S$. Instrumental isotopic mass fractionation is monitored with the $^{34}S/^{32}S$ ratio such that

$$\delta^{34}S = \left[\frac{(^{34}S/^{32}S)_{measured}}{(^{34}S/^{32}S)_{standard}} - 1\right] \times 1000$$

where $(^{34}S/^{32}S)_{measured}$ is the measured $^{34}S^-/^{32}S^-$ ratio, $(^{34}S/^{32}S)_{standard}$ is the reference value based on the mean of the standards measured, and $\delta^{34}S$ is expressed in permil (‰). A similar formulation is used for $\delta^{33}S$ and $\delta^{36}S$. For mass dependent fractionation the expected isotope ratios of $^{33}S/^{32}S$ and $^{36}S/^{32}S$ can be calculated from the measured $\delta^{34}S$, with the deviation of the measured ratios from that expected expressed as

$$\Delta^{33}S = \delta^{33}S - \delta^{34}S \times 0.515$$

$$\Delta^{36}S = \delta^{36}S - \delta^{34}S \times 1.90$$

The mass fractionation factors 0.515 and 1.90 have been determined theoretically and experimentally for mass dependent fractionation [14]. For samples showing mass dependent fractionation alone, the values of $\Delta^{33}S$ and $\Delta^{36}S$ should be close to zero.

Our experiments include analysis of the commonly used pyrite standards Ruttan and Balmat [15]. These pyrites have notably different S isotopic compositions with $\delta^{34}S$ being +1.2‰ for Ruttan and +15.1‰ for Balmat. This large difference in composition provides an excellent test of the capability of our analytical protocols, not only for the determination of $\delta^{34}S$ but for $\Delta^{33}S$ and $\Delta^{36}S$ at markedly different values of $\delta^{34}S$. $\Delta^{33}S$ and $\Delta^{36}S$ have not been measured conventionally for these samples, but their compositions are determined to be close to zero on the basis of extensive ion microprobe measurements [16].

The analytical protocol follows that outlined above involving rastering and pre-sputtering of the spot. $^{32}S^-$ is collected on a 10^{11} Ω resistor, $^{33}S^-$ and $^{34}S^-$ on 10^{12} Ω resistors, and $^{36}S^-$ by charge mode. For the sulfur four-isotope measurements, a set consisted of 6 scans of 20 s, and the analysis comprised 6 sets, with a total integration time of 720 s (12 min). In the course of an analysis, the S^- secondary-ion beam shows strong in-growth with the $^{32}S^-$ count rate starting at around 700 MHz ($^{36}S^-$ set to 100,000 c/s) and finishing at 1500 MHz. The $^{34}S/^{32}S$ is also seen to systematically rise along with the count rate. The scans in the first set are generally within counting statistic error of each other (set error of ca. 0.05‰). The total uncertainty only increases with the addition of data from the succeeding five sets and is consistent with the systematic change in the $^{34}S^-/^{32}S^-$ during the course of an analysis. For the purposes of this work, we use only the first set for the determination of $\delta^{34}S$. For the calculation of $\Delta^{33}S$ and $\Delta^{36}S$, the data are evaluated on a scan by scan basis, i.e. the $\delta^{33}S$ and $\delta^{36}S$ are normalized from the $\delta^{34}S$ for each scan, thereby obtaining 36 estimates of $\Delta^{33}S$ and $\Delta^{36}S$. The values of $\Delta^{33}S$ and $\Delta^{36}S$ are the means of the 36 individual estimates. Analyses are normalized to the Ruttan measurements such that the mean Ruttan $\delta^{34}S$ is +1.2‰ [15]; while $\Delta^{33}S$ and $\Delta^{36}S$ are assumed to be zero. The measurement errors of $\Delta^{33}S$ and $\Delta^{36}S$ are based on the standard errors of the means of $\Delta^{33}S$ and $\Delta^{36}S$.

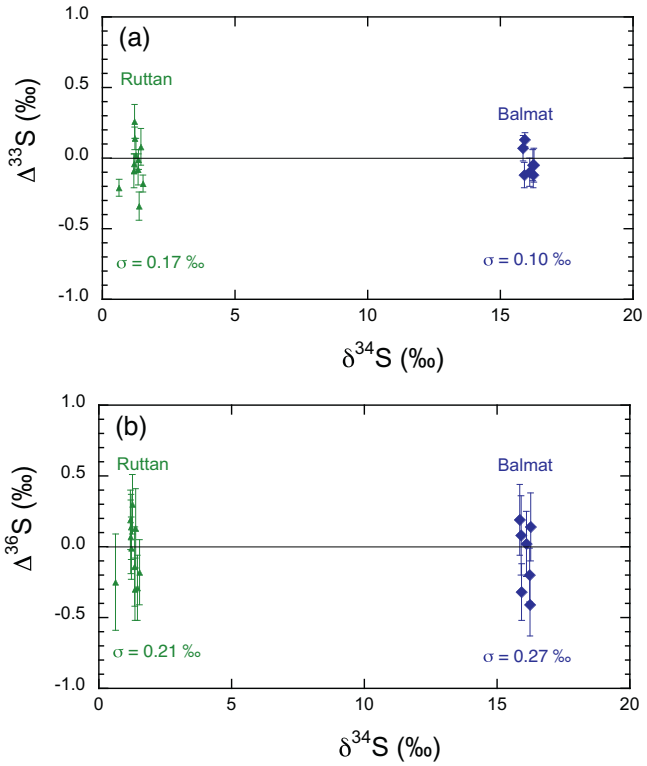

Fig. 6. Sulfur four-isotope compositions of Balmat and Ruttan standards (a) $\Delta^{33}S$ vs $\delta^{34}S$ and (b) $\Delta^{36}S$ vs $\delta^{34}S$ for Balmat and Ruttan pyrites. $\delta^{34}S$ is normalized to a value of +1.2‰ for Ruttan [15]. $\Delta^{33}S$ and $\Delta^{36}S$ are normalized to zero for Ruttan. $^{32}S^-$ collected across 10^{11} Ω resistor, $^{33}S^-$ and $^{34}S^-$ across 10^{12} Ω resistors, and $^{36}S^-$ by charge mode on a 22 pF capacitor; count rate was initially set for $^{36}S^-$ of 100,000 c/s.

Data are presented in Table 2 and Fig. 6. $\delta^{34}S$ is normalized to the mean of the Ruttan analyses being +1.2‰. The standard deviation of all analyses is 0.23‰ and the standard error is 0.07‰. One analysis (#3.1) could be an outlier but makes a difference of only 0.1‰ to the mean if it is excluded; this is inconsequential to the determinations of mass dependent fractionation. As expected Balmat is heavier at ca. +16.0‰ with a standard deviation of 0.18‰ and standard error of 0.07‰. This is slightly heavier than found by Crowe and Vaughan [15] but consistent with the determinations of Whitehouse [16].

$\Delta^{33}S$ has been normalized to effect a mean of the Ruttan analyses at 0.00‰. The standard deviation is 0.17‰ and the standard

Table 2
Sulfur 4-isotope measurements.

	$\delta^{34}S$ (‰)[a]	$\delta^{33}S$ (‰)	$\Delta^{33}S$ (‰)[b]	$\pm\Delta^{33}S$ (‰)	$\delta^{36}S$ (‰)	$\Delta^{36}S$ (‰)[b]	$\pm\Delta^{36}S$ (‰)
Ruttan							
3.1	0.58	0.12	−0.17	0.03	0.95	−0.22	0.17
3.2	1.14	0.52	−0.05	0.06	2.46	0.22	0.10
1.3	1.16	0.88	0.30	0.06	2.43	0.17	0.12
1.4	1.40	0.83	0.12	0.06	2.47	−0.26	0.11
1.5	1.48	0.61	−0.14	0.03	2.72	−0.15	0.11
1.6	1.30	0.61	−0.04	0.06	2.42	−0.11	0.14
1.7	1.31	0.69	0.03	0.03	2.29	−0.27	0.11
1.8	1.21	0.67	0.06	0.06	2.70	0.33	0.10
3.3	1.17	0.77	0.18	0.04	2.32	0.02	0.11
1.1	1.15	0.57	0.00	0.04	2.35	0.10	0.13
1.11	1.33	0.37	−0.30	0.05	2.75	0.16	0.14
Mean	1.20	0.60	−0.00		2.35	0.00	
Std dev	0.23	0.21	0.17		0.49	0.21	
Std err	0.07	0.07	0.05		0.20	0.07	
Balmat							
3.1	15.80	8.21	0.11	0.05	30.53	0.22	0.12
3.3	15.87	8.30	0.17	0.02	30.15	−0.29	0.10
2.1	16.17	8.26	−0.01	0.05	30.83	−0.17	0.10
1.4	16.05	8.16	−0.06	0.05	30.82	0.05	0.11
1.5	16.21	8.29	−0.01	0.06	31.26	0.17	0.12
2.2	15.85	8.04	−0.08	0.05	30.49	0.11	0.14
2.3	16.19	8.21	−0.08	0.05	30.68	−0.38	0.11
Mean	16.02	8.21	0.01		30.68	−0.04	
Std dev	0.18	0.09	0.10		0.35	0.27	
Std err	0.07	0.04	0.04		0.11	0.13	

All measurement errors are 1σ.
[a] Normalized to Ruttan $\delta^{34}S = +1.20$‰.
[b] Normalized to Ruttan $\Delta^{33}S = 0$, $\Delta^{36}S = 0$.

error is 0.05‰. In comparison, the weighted mean $\Delta^{33}S$ of Ruttan based on this normalization is -0.08 ± 0.03 with an MSWD of 3.3 suggesting that the errors are likely underestimated if this is a homogeneous material and the analyses are normally distributed. Similarly $\Delta^{36}S$ has been normalized to effect a mean of the Ruttan analyses at 0.00‰. The standard deviation is 0.21‰ and the standard error is 0.07‰. In comparison, the weighted mean of Ruttan based on this normalization is -0.01 ± 0.07 with an MSWD of 0.83, indicating a good correspondence of measurement errors and the distribution of the data.

The mean value of Balmat $\Delta^{33}S$ is 0.01 with a standard deviation of 0.10‰ and standard error of 0.04‰. The weighted mean $\Delta^{33}S$ is 0.01 ± 0.03‰ with an MSWD of 2.0 suggesting a slight degree of excess scatter. The mean value of Balmat $\Delta^{36}S$ is −0.04 with a standard deviation of 0.27‰ and standard error of 0.13‰. The weighted mean $\Delta^{36}S$ is -0.11 ± 0.09‰ with an MSWD of 0.83, indicating a good correspondence of measurement errors and the distribution of the data.

The Balmat and Ruttan data are consistent with them having the same $\Delta^{33}S$ and $\Delta^{36}S$ values. However, we have no certified standard for $\Delta^{33}S$ and $\Delta^{36}S$ and so the specific values must await further analysis. However, the data shown by Whitehouse [16] indicates that $\Delta^{33}S$ and $\Delta^{36}S$ for Balmat are close to zero.

The $\Delta^{36}S$ data from Ruttan and Balmat shows precision that we calculate is only a factor of two above that expected from counting statistics, and is in accord with the additional thermal noise predicted for the capacitor-based detector (see Fig. 2). As such, the system is performing close to the theoretical limit. This is highly encouraging and allows us to forgo our electron multiplier system for isotopic measurements involving ion beams with signal intensity down to 100,000 c/s. At this stage we have not pursued isotope ratio measurements at lower effective count rates.

The $\Delta^{33}S$ performance is perhaps not as good as it should be given the $\Delta^{36}S$ data. The $^{33}S^{-}$ beam is nearly a factor of 50 higher than $^{36}S^{-}$ yet $\Delta^{33}S$ is only marginally more precise than $\Delta^{36}S$. There are a number of possible contributors to this behavior. Probably the main issue is that this detector head was inserted into a fixed position in the collector chamber. The head can be maneuvered, but only by breaking vacuum and manually adjusting its position. As such, it may not be exactly in the optimum position for any given measurement. The ^{33}S–^{34}S distance is effectively fixed in this system, and any lens adjustment of the secondary beam can cause slight changes in dispersion that can only be accommodated within a certain range. Another issue for this system is the connection of the Faraday cup to the electrometer. While the other heads have fully shielded solid lead throughs, the ^{33}S head is simply connected by wire to a vacuum feedthrough holding the electrometer. It is possible that some degree of noise could be caused through this suboptimal linkage. On the other hand, the $\Delta^{33}S$ data is still reproducing at the 0.1‰ level and for a system where there is many permil variation (e.g. [8]), it is already performing adequately for many geological applications. Further refinement of $\Delta^{33}S$ measurements will follow a redevelopment of the multiple collector to include five, movable, solid-feed-through heads.

4. Discussion

4.1. Ion microprobe measurements

Multiple-collection measurement on ion microprobes has seen significant advances in the recent past. Multiple Faraday systems are used for stable isotope analysis where isotopic signals (for O and S) are generally sufficiently high to use multiple Faraday cups in current mode and achieve sub-permil precision in analytical times of only a few minutes. Multiple collections have a major benefit in effectively canceling noise associated with instability in the primary beam. The internal analytical precision for ion microprobe analysis with multiple Faraday cups can be of the order of 0.05‰ for appropriate secondary ion signal strengths, although external reproducibility is probably at least a factor of three higher. Given the well-known variability in instrumental mass fractionation with different paths through the ion optics [17]

it is quite difficult to ascertain what part of the external reproducibility is related to the detector system and what might be related to instrumental conditions. Nevertheless, determinations of mass-dependent fractionation with isotopic measurements on current-mode electrometers are better than 0.3‰ and are routine in isotope geochemistry.

A major area of advancement in recent times has involved the measurement of minor isotopes in stable isotope systems (e.g. ^{17}O, ^{33}S, ^{36}S). The abundances of these isotopes are assessed relative to mass fractionation laws and any deviations are referred to as mass independent fractionation (MIF). MIF is perhaps a bit of a misnomer because seldom are mass-dependent and mass-independent fractionations mutually exclusive, but the measurement of these minor isotopes provides a tool with which to examine geological processes. The determination of the abundance of ^{17}O has been important in terms of cosmochemistry with variation in the abundance of ^{16}O causing correlated variation in $\delta^{17}O$ and $\delta^{18}O$ [18]. The abundances of ^{33}S and ^{36}S are finding increasing application in terms of deciphering biologic activity vs photochemical reactions in the Archean atmosphere [14,19]. These measurements are of particular interest in ion microprobe analysis because spatial context can be maintained. Moreover, the determinations of the residuals $\Delta^{17}O$, $\Delta^{33}S$, and $\Delta^{36}S$ are independent of mass dependent fractionation and therefore should be absolute determinations. The precision of these measurements is not limited by the reproducibility of the standard as is the case for mass-dependent fractionation measurements. Of these minor isotopes, measurements of ^{17}O and ^{36}S are the most difficult because current-mode electrometers are compromised by the background signals. Furthermore, an ongoing goal in geochemistry is to measure higher precision in smaller analytical volumes. But as the analytical volume gets smaller so the number of ions available for measurement will fall.

Therefore the ability to measure isotope ratios over a continuous range of beam strengths is an important issue in the progression of ion microprobe measurements. In the following section, we evaluate the performance of the SHRIMP SI counting system for sulfur isotopic analysis and the ramifications for isotope ratio measurements over a wide range of signal intensities.

4.2. Ion beam measurements

4.2.1. Electron multiplier measurement

Sulfur-isotope data collected on the electron multiplier system is disappointing to say the least. One of the key design goals was to incorporate large high-performance ETP multipliers into the detector system with a perceived benefit of better gain stability than the CDEM used on the SHRIMP II multiple collectors. During the course of these experiments we have found substantial drift in the gain of the multiplier. The drift is worse at 300,000 c/s and is lessened with a count rate of 50,000 c/s. Therefore, this drift appears to be proportional to the number of counts generated by the multiplier. This characteristic has also been found on Cameca 1280 instruments during $^{36}S^-$ measurements [16,20]. In these studies the drift was ameliorated by increasing the potential on the electron multiplier dynode chain at a rate proportional to the count rate on the multiplier although gain drift corrections were still required. As correctly pointed out by Farquhar et al. [20] the drift correction requires the propagation of an uncertainty on to the measurement further decreasing the attainable precision.

However, we also find that the reproducibility of the measurements is not consistent with the measurement errors even at the low count rate. These data tend to show a slight downward drift overall, but the data show excess scatter about the drift trend. We suspect that this characteristic is due to the secondary beam hitting the conversion dynode at slightly different positions which is affecting the signal from the multiplier. If the beam hits an area of the dynode that has experienced a different exposure history, then this will cause a change in the response and potentially a change in the instrumental mass fractionation. This inference is supported by recent work using a Cameca 1280 [20] where the primary beam was rastered over an area to provide a stable $^{36}S^-$ beam on the electron multiplier. Another method for desensitizing positional sensitivity of the detector system is by scanning the beam across the dynode. However, placing a scanning device between the slit and conversion dynode on the SHRIMP SI multicollector was not envisaged during the design phase of SHRIMP SI.

As noted in the introduction of this paper, getting optimum performance from pulse counting systems has proven to be difficult. In many cases, the operation of an ion counting system at low count rates can effectively mask issues because the precision per unit time is quite low. For single collection, the gain drift is not of particular concern because the highest intensity peaks are only collected for a short period of time. There is cause for concern however, when high count rates are required for an extended period of time and even for count rates that we would consider moderate, i.e. 100,000 c/s. Previously we have suspected that the induced gain drift is species specific. We have noted that S analysis (even as S^+) causes drift in an electron multiplier at a greater rate compared to the peaks used in U–Pb geochronology measurements [21]. The electron multiplier system on SHRIMP SI uses a conversion dynode and only secondary electrons from the conversion dynode are triggering the multiplier. If sulfur poisoning of the detector is an issue, then it is occurring on the conversion dynode and changing the gain on the multiplier is compensating for fewer electrons, or lower energy electrons. It should also be noted that this is a result for a specific type of electron multiplier and other types could have a different response and may not show the same degradation rate. Nevertheless, the characteristics of electron multipliers need to be examined closely in the context of the count rates that are required for an analysis.

4.2.2. Electrometer current mode

The standard configuration of a Faraday cup – electrometer involves the measurement of the feedback current through a high-ohmic resistor. This configuration works well in nearly all mass spectrometers involved in high precision measurement of nominally high ion beam intensity [22]. For the measurements presented here, $^{32}S^-$ can be measured across a 10^{11} Ω resistor and $^{34}S^-$ across a 10^{12} Ω resistor. For these measurements the uncertainty in the background contributes mainly to the $^{34}S^-$ measurement with the lower signal intensity. With the highest available signal intensities isotope ratios reproduce at the 0.2‰ level, allowing calculation of standard errors in the mean at the 0.1‰ level or better. For $\delta^{34}S$, the uncertainty is mainly in the $^{34}S^-$ determination. Counting statistics predict an uncertainty at the level of 0.075‰ for an analysis, although this cannot be achieved in the current experiments because of the change in instrumental mass fractionation during the course of an analysis.

4.2.3. Electrometer charge mode

Our data show that the charge mode measurements of $^{36}S^-$ produce $\Delta^{36}S^-$ values that are consistent within measurement uncertainties of ca. 0.2‰. There is no indication of drift in the data and the assigned measurement uncertainties appear to be appropriate indicators of the precision of an analysis. In comparison, the $\Delta^{33}S$ values (with $^{33}S^-$ determined across the 10^{12} Ω resistor) appear to show scatter in excess of that predicted from the measurement errors. It is unclear whether there is a noise component affecting $^{33}S^-$ alone, or whether this might be affecting all sulfur isotope ratios at the 0.1‰ level. A further consideration would be the homogeneity of the standards since we assume that the $\delta^{34}S$ is representative of the whole analysis and small artifacts could be produced if this is changing. However, the point of this

exercise is not a full assessment of analytical uncertainties in sulfur isotope analyses of geological materials; this will await further work. Rather the issue here is to demonstrate the great promise that charge mode collection has for S isotopic analysis and for any isotopic system where count rates around the 100,000 c/s level require quantification.

A major advantage of charge mode is that the same detection system can be used from count rates of over 10^9 c/s down to 10^5 c/s. That is, the same Faraday cup system used for current-mode acquisition can be used for charge mode with the mode change being no different to switching resistors in the electrometer. In many cases this removes the requirement of having to move to an electron-multiplier-based pulse-counting system for measurements at this signal strength. Finally, an additional benefit of not using an electron multiplier is a more pragmatic one. Electron multipliers have a finite life time and are moderately expensive to replace. Collecting secondary ions in a Faraday cup shows no such degradation.

5. Conclusions

Charge-mode has long been recognized as a potential extension of Faraday cup measurements enabling measurements at count rates regarded as within the domain of electron multipliers. However, implementation of charge mode has not been straightforward and has required attention to details of rigidity of mounting, electrical contacts, and signal processing. The data collected in these experiments demonstrate that charge-mode data collection is practical for isotope-ratio measurements on a secondary ion mass spectrometer, and it is likely a practical development on other types of mass spectrometer.

Acknowledgements

JA holds a fellowship awarded by the Australian Government's Enterprise Connect – Researcher in Business Program, which is supported by Australian Scientific Instruments and the Research School of Earth Sciences, ANU.

The iFlex electrometer was designed and constructed at the Research School of Earth Sciences Electronics Workshop.

The building of SHRIMP SI would not have been possible without an Australian Research Council – Linkage Instrumentation Equipment Fund grant, with the support of University of Tasmania, The University of Queensland, Curtin University, University of Wollongong, The University of Melbourne, CSIRO, Geoscience Australia, and Australian Scientific Instruments. Sulfur isotope measurements on SHRIMP SI are supported by ARC DP140103393.

References

[1] Keithley Instruments, Low Level Measurements Handbook, Keithley Corporation, 2004, pp. 244.
[2] J. Koornneef, C. Bouman, J. Schwieters, G. Davies, Use of 10^{12} and 10^{13} ohm resistors in TIMS analysis of Sr and Nd isotopes in sub-nanogram geological and environmental samples, Mineralogical Magazine 77 (2013) 1495.
[3] J.M. Hayes, D.A. Schoeller, High precision pulse counting: limitations and optimal conditions, Analytical Chemistry 49 (1977) 306–311.
[4] R. Sarpeshkar, T. Delbrück, C.A. Mead, White noise in MOS transistors and resistors, IEEE Circuits and Devices Magazine 9 (1993) 23–29.
[5] T.M. Esat, Charge collection thermal ionization mass spectrometry of thorium, International Journal of Mass Spectrometry and Ion Processes 148 (1995) 159–170.
[6] T.B. Coplen, J.K. Böhlke, P. De Bièvre, T. Ding, N.E. Holden, J.A. Hopple, H.R. Krouse, A. Lamberty, H.S. Peiser, K. Revesz, S.E. Rieder, K.J.R. Rosman, E. Roth, P.D.P. Taylor, R.D.J. Vocke, Y.K. Xiao, Isotope-abundance variations of selected elements (IUPAC Technical Report), Pure and Applied Chemistry 74 (2002) 1987–2017.
[7] S.J. Mojzsis, C.D. Coath, J.P. Greenwood, K.D. McKeegan, T.M. Harrison, Mass-independent isotope effects in Archean (2.5 to 3.8 Ga) sedimentary sulfides determined by ion microprobe analysis, Geochimica et Cosmochimica Acta 67 (2003) 1635–1658.
[8] Y. Xue, I. Campbell, T.R. Ireland, P. Holden, R. Armstrong, No mass-independent sulfur isotope fractionation in auriferous fluids supports a magmatic origin for Archean gold deposits, Geology 41 (2013) 791–794.
[9] T.R. Ireland, S. Clement, W. Compston, J.J. Foster, P. Holden, B. Jenkins, P. Lanc, N. Schram, I.S. Williams, Development of SHRIMP, Australian Journal of Earth Sciences 55 (2008) 937–954.
[10] H. Matsuda, Double focusing mass spectrometers of second order, International Journal of Mass Spectrometry and Ion Physics 14 (1974) 219–233.
[11] M. Dodson, A linear method for second-degree interpolation in cyclical data collection, Journal of Physics E: Scientific Instruments 11 (1978) 296.
[12] E. Zinner, A.J. Fahey, K.D. McKeegan, Characterization of electron multipliers by charge distributions, in: A. Benninghoven, R. Colton, D. Simons, H. Werner (Eds.), Secondary Ion Mass Spectrometry SIMS V, Springer, Berlin, Heidelberg, 1986, pp. 170–172.
[13] P. Holden, P. Lanc, T.R. Ireland, T.M. Harrison, J.J. Foster, Z. Bruce, Mass-spectrometric mining of Hadean zircons by automated SHRIMP multi-collector and single-collector U/Pb zircon age dating: the first 100,000 grains, International Journal of Mass Spectrometry 286 (2009) 53–63.
[14] S. Ono, B. Wing, D. Johnston, J. Farquhar, D. Rumble, Mass-dependent fractionation of quadruple stable sulfur isotope system as a new tracer of sulfur biogeochemical cycles, Geochimica et Cosmochimica Acta 70 (2006) 2238–2252.
[15] D.E. Crowe, R.G. Vaughan, Characterization and use of isotopically homogeneous standards for in situ laser microprobe analysis of $^{34}S/^{32}S$ ratios, American Mineralogist 81 (1996) 187–193.
[16] M.J. Whitehouse, Multiple sulfur isotope determination by sims: evaluation of reference sulfides for $\Delta^{33}S$ with observations and a case study on the determination of $\Delta^{36}S$, Geostandards and Geoanalytical Research 37 (2013) 19–33.
[17] N. Shimizu, S.R. Hart, Isotope fractionation in secondary ion mass spectrometry, Journal of Applied Physics 53 (1982) 1303–1311.
[18] T.R. Ireland, Oxygen isotope tracing of the solar system, Australian Journal of Earth Sciences 59 (2012) 225–236.
[19] J. Farquhar, H.M. Bao, M. Thiemens, Atmospheric influence of earth's earliest sulfur cycle, Science 289 (2000) 756–758.
[20] J. Farquhar, J. Cliff, A.L. Zerkle, A. Kamyshny, S.W. Poulton, M. Claire, D. Adams, B. Harms, Pathways for Neoarchean pyrite formation constrained by mass-independent sulfur isotopes, Proceedings of the National Academy of Sciences of the United States of America 110 (2013) 17638–17643.
[21] C.S. Eldridge, W. Compston, I.S. Williams, J.L. Walshe, R.A. Both, In situ micro-analysis for $^{34}S/^{32}S$ ratios using the ion microprobe SHRIMP, International Journal of Mass Spectrometry and Ion Processes 76 (1987) 65–83.
[22] T.R. Ireland, Recent developments in isotope-ratio mass spectrometry for geochemistry and cosmochemistry, Review of Scientific Instruments 84 (2013) 011101–011121.